

# Journal of Astronomical Telescopes, Instruments, and Systems

AstronomicalTelescopes.SPIEDigitalLibrary.org

## Integration of a ${}^6\text{LiInSe}_2$ thermal neutron detector into a CubeSat instrument

Joanna C. Egner  
Michael Groza  
Arnold Burger  
Keivan G. Stassun  
Vladimir Buliga  
Liviu Matei  
Julia G. Bodnarik  
Ashley C. Stowe  
Thomas H. Prettyman

**SPIE.**

Joanna C. Egner, Michael Groza, Arnold Burger, Keivan G. Stassun, Vladimir Buliga, Liviu Matei, Julia G. Bodnarik, Ashley C. Stowe, Thomas H. Prettyman, "Integration of a  ${}^6\text{LiInSe}_2$  thermal neutron detector into a CubeSat instrument," *J. Astron. Telesc. Instrum. Syst.* **2**(4), 046001 (2016), doi: 10.1117/1.JATIS.2.4.046001.

# Integration of a ${}^6\text{LiInSe}_2$ thermal neutron detector into a CubeSat instrument

Joanna C. Egner,<sup>a,b,\*</sup> Michael Groza,<sup>b</sup> Arnold Burger,<sup>a,b</sup> Keivan G. Stassun,<sup>a,b</sup> Vladimir Buliga,<sup>b</sup> Liviu Matei,<sup>b</sup> Julia G. Bodnarik,<sup>c</sup> Ashley C. Stowe,<sup>a,d</sup> and Thomas H. Prettyman<sup>e</sup>

<sup>a</sup>Vanderbilt University, Department of Physics and Astronomy, 2401 Vanderbilt Place, Nashville, Tennessee 37240, United States

<sup>b</sup>Fisk University, Fisk Vanderbilt Bridge Program, Department of Physics, Material Science and Application Group, 1000 17th Avenue North, Nashville, Tennessee 37208, United States

<sup>c</sup>University of Arizona, Lunar and Planetary Laboratory, 1629 East University Boulevard, Tucson, Arizona 85721, United States

<sup>d</sup>Y-12 National Security Complex, 602 Scarboro Road, Oak Ridge, Tennessee 37830, United States

<sup>e</sup>Planetary Science Institute, 1700 East Fort Lowell Road #106, Tucson, Arizona 85719, United States

**Abstract.** We present a preliminary design for a neutron detection system that is compact, lightweight, and low power consuming, utilizing the CubeSat platform making it suitable for space-based applications. This is made possible using the scintillating crystal lithium indium diselenide ( ${}^6\text{LiInSe}_2$ ), the first crystal to include  ${}^6\text{Li}$  in the crystalline structure, and a silicon avalanche photodiode. The schematics of this instrument are presented as well as the response of the instrument to initial testing under alpha radiation. A principal aim of this work is to demonstrate the feasibility of such a neutron detection system within a CubeSat platform. The entire end-to-end system presented here is  $10 \times 10 \times 15 \text{ cm}^3$ , weighs 670 g, and requires 5 V direct current at 3 W. © 2016 Society of Photo-Optical Instrumentation Engineers (SPIE) [DOI: [10.1117/1.JATIS.2.4.046001](https://doi.org/10.1117/1.JATIS.2.4.046001)]

Keywords: neutron detection instrument; CubeSat; scintillator; avalanche photodiode.

Paper 16024 received Apr. 1, 2016; accepted for publication Oct. 19, 2016; published online Nov. 8, 2016.

## 1 Introduction

There is a growing interest in the characterization of near-Earth objects such as the moon, asteroids, and planets due to an expansion of investigation of the extra-terrestrial for both scientific and economic purposes. Characterization includes the investigation of these objects' bulk composition in effort to better understand the chemistry of the subsurface, which in turn could give constraints on solar system formation theories and furthermore provides potentially valuable commercial information such as asteroid mining. Previous nuclear measurements have primarily given information regarding the composition of the top-most surface layer, on the order of about 10 cm.<sup>1</sup> While the characterization of the surface of objects is valuable, often the surface and bulk compositions are very different because of exposure and weathering effects that predominantly affect the surface such as ionization from the sun, the evaporation of liquids due to low surface gravity or lack of atmosphere, and erosion from cosmic wind.<sup>2</sup>

Historically, the classification of asteroids has been carried out by optical albedo observations, measuring the scintillation spectrum of light that they give off.<sup>3</sup> However, because the bulk and surface composition can differ greatly, albedo measurements are not always the most accurate way of determining the composition of the bulk of the asteroid. With the development of a better system of elemental detection, classification could be done much more accurately. Not only would this provide important information that could help answer questions pertaining to the origin and distribution of asteroids, it would also have major implications in the developing sector of asteroid

mining by making the classification and identification of the best candidates for mining easier and more accurate. A lithium indium diselenide ( ${}^6\text{LiInSe}_2$ )-based CubeSat instrument will have the capability to probe to depths of 50 cm below the surface of solar system bodies, while weighing and consuming a fraction of the weight and power of the traditional instruments described in the literature.<sup>1,4–7</sup> The use of neutron detectors will be a major component in studies of the chemical composition of asteroids and planets.

Previously, all neutron-detecting instruments have been large and require high voltage. Therefore, it would have been impossible to package one of these detectors in the boundaries of the CubeSat platform. Examples of neutron detectors included on previous missions include the Helium-3 tube detector included in the 1998 Lunar Prospector, the boron-loaded plastic scintillator included in the 2001 Mars Odyssey mission, and the 2007 gamma ray and neutron detector (GRaND) Dawn mission to explore Ceres and Vesta which utilized boron-loaded plastic and lithium-loaded glass scintillators, as well as a semiconducting cadmium zinc tellurium (CdZnTe) crystal array.<sup>5,6,8</sup> These instruments are both heavy and have high power requirements: 30 kg, 32 W for Mars Odyssey and 10 kg, 15 W for GRaND.<sup>5,8</sup> While  ${}^3\text{He}$  gas tubes are highly efficient neutron detectors due to a high cross-section for neutron detection, they are heavy, require high voltage, and are bulky. Similarly, most scintillator-based detectors require pairing with photomultiplier tube (PMT) systems, which are sensitive to magnetic fields, add weight to payload, and increase power consumption. Therefore, there is great interest in developing a solid-state neutron detector that is more compact, requires less power, and does not have

\*Address all correspondence to: Joanna C. Egner, E-mail: [joannaegner@gmail.com](mailto:joannaegner@gmail.com)

sensitivity to magnetic fields to implement into a cost-effective space instrument.

${}^6\text{Li}$  has a large cross-section, 940 barns, for thermal neutron capture following the reaction  ${}^6\text{Li} + {}^1_0\text{n} \rightarrow {}^7\text{Li}^* \rightarrow {}^4\text{He}(2.056 \text{ MeV}) + {}^3\text{H}(2.729 \text{ MeV})$ , the  $Q$ -value, or the energy released, depends on the energy liberated following the neutron capture and in this case is 4.785 MeV.<sup>9</sup> Traditionally,  ${}^6\text{Li}$  is used as an absorber on semiconductors to increase efficiency, but  ${}^6\text{LiInSe}_2$  is the first semiconductor to have  ${}^6\text{Li}$  in the structure of the crystal. It can be operated as either a semiconductor or a scintillator; at the current state of development and purification,  ${}^6\text{LiInSe}_2$  is more efficient to use as scintillator.<sup>10-12</sup> Since  ${}^6\text{LiInSe}_2$  can be used in either semiconductor or scintillator mode, one of the initial decisions we had to make was the preferred mode of operation for the CubeSat prototype. We have found that, at the present level of material development, the signal-to-noise ratio is improved by 42% in the scintillator mode of operation.

The development of a lithium indium diselenide  ${}^6\text{LiInSe}_2$ <sup>10</sup> thermal neutron sensor is especially attractive because of its ability to be spectrally matched (510 nm emission) with newly developed silicon-based photodetectors such as silicon avalanche photodiodes (Si-APD) and silicon photomultipliers (SiPM), that can be used in place of traditional PMTs. These are much less bulky and heavy, and have the potential to be packaged into a compact, lightweight, low power detector system. Comparing models from manufacturer Hamamatsu Photonics, their SiPM has a mass of 1 g and their PMT has a mass of 100 g, while the SiPM is also 10% smaller.

In this paper, the prototype of a neutron detection CubeSat system and the preliminary performance tests that demonstrate the ability to deploy a neutron detection instrument in a compact footprint are discussed. The prototype combines the innovative technology of  ${}^6\text{LiInSe}_2$  and an Si-APD. This pairing eliminates the need for a conventional PMT making it possible to package this instrument under the restrictions of the CubeSat program. Section 2 describes the design of the instrument and briefly discusses each component as well as the reasoning behind the selections. Section 3 presents preliminary results and the basics of the instrument functions.

## 2 Instrument Design

### 2.1 CubeSat Design Specifications

NASA's CubeSat Launch Initiative is a platform that allows researchers to compete for flight opportunities to conduct low-cost space science experiments. Instruments can be from 1 to 6 units (U), with some subincrements of 0.5 units available, with specific weight, size, and power requirements that can be found in Ref. 13. The criteria for a 1.5U include the size of  $10 \times 10 \times 15 \text{ cm}^3$ , a weight limit of 2.00 kg (4.4 lbs), and a requirement to run off the power supplied by onboard solar panels or batteries.<sup>13</sup> The 0.5U IRIS Deep Space Transponder CubeSat, built by JPL, has a power consumption of 26 W during full power transmission, and the 6U JPL MarCO, has a power consumption of 35 W.<sup>14,15</sup>

### 2.2 CubeSat Design

In the development of our instrument, we have utilized a 1.5-U CubeSat chassis. A block diagram of the instrument is shown in Fig. 1. In this figure, the active area of the detector, the encapsulated  ${}^6\text{LiInSe}_2$  crystal, is oriented to be at the top. A thermal neutron interacts with the  ${}^6\text{Li}$  nucleus, and the resulting nuclear reaction generates an energetic alpha particle that in an ionization cascade generates excited states in the scintillator crystal that ultimately recombine to their ground state by emitting optical photons.<sup>9</sup> The scintillating photons are then detected by the Si-APD and converted into an electronic signal, or pulse, that is further processed to generate a histogram of all events that constitute the spectrum of incoming radiation. In general, neutron detection takes place in a mixed field of other ionizing particles such as gamma and galactic cosmic rays and the characteristics of the pulse can be used to discriminate among types of particles interacting with the detector.

Figure 1 shows the schematic of our instrument. The instrument has three stages, comprised of a printed circuit board (labeled boards 1, 2, and 3 in all figures) and the associated components. The first board contains the  $9 \times 9 \times 2 \text{ mm}^3$   ${}^6\text{LiInSe}_2$ -encapsulated crystal and the Si-APD (components 1 and 2 in all figures), which have been packaged together to prevent the crystal from shifting off the active area of the

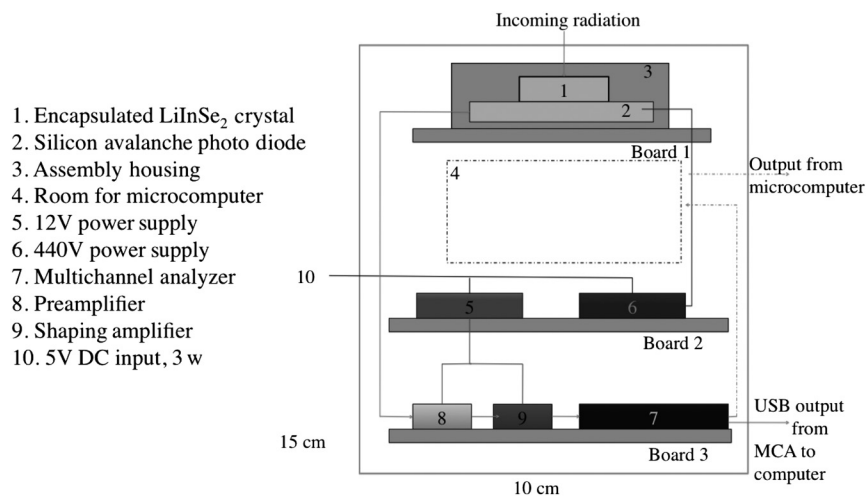
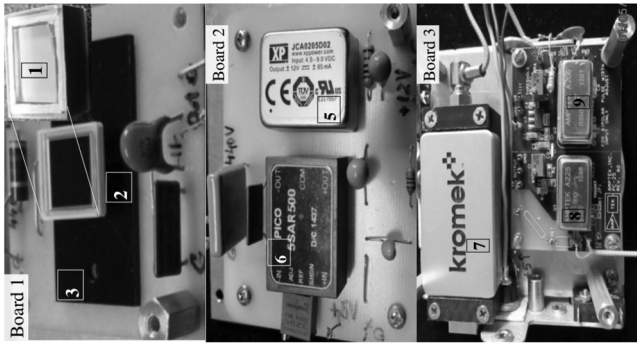


Fig. 1 Neutron CubeSat prototype schematic.



**Fig. 2** Photo of associated electronics. Labeling of components is the same as the one used in Fig. 1.

Si-APD that is slightly larger than the crystal at  $10 \times 10 \text{ mm}^2$ . Packaging the crystal and Si-APD together also decreases the amount of ambient light that can reach the Si-APD. Board 2 contains two DC-DC regulated power supplies (components 5 and 6) that convert the 5 V input to the instrument into 12 and 440 V, respectively. The 440-V power supply powers the Si-APD, while the 12-V supply runs the remaining components, the two amplifiers and the Kromek multichannel analyzer (MCA). The third board contains a preamplifier and shaper (component 8), a voltage amplifier (component 9), and the MCA (component 7), which currently, for lab tests, outputs via USB cable to a computer. There is room as well as weight and power available for a microcomputer and wireless transmitter to be included in a later iteration of the instrument, although a RaspberryPi is being used in initial tests. The current instrument, including the RaspberryPi microcomputer, weighs 670 g in its entirety and requires 5 V and 3 W.

The  ${}^6\text{LiInSe}_2$  crystal being used in the detector was grown using the vertical Bridgman method with details of growth being given by Tupytsin et al. and using a technology that was developed through a partnership between Fisk University and Y-12 National Security Complex.<sup>10</sup>  ${}^6\text{Li}$  is a high-density material suitable for producing lightweight and compact neutron detectors

due to its high capture cross-section for thermal neutrons.  ${}^6\text{Li}$  and other neutron sensitive materials are traditionally used as coatings on neutron-detecting systems to increase the efficiency to a total of a few percent. In comparison, the density of  ${}^6\text{Li}$  in  ${}^6\text{LiInSe}_2$  is great enough to yield up to 95% detection efficiency of neutrons in a 3.4-mm-thick wafer.<sup>11</sup>

The  ${}^6\text{LiInSe}_2$  crystal utilized in the detector is  $9 \times 9 \times 2 \text{ mm}^3$ . After characterization and testing, discussed more in Sec. 3, it was encapsulated, covered on five sides with reflective material with a quartz window on the sixth side as shown in the topmost panel of Fig. 2 labeled 1. This side was then placed onto the Si-APD.

The photodetector, in this case the Si-APD (component 2), turns detected events into electrical pulses. Compared to Si-APDs and SiPMs, traditional vacuum PMTs are heavy, large, have high power requirements, and are sensitive to the magnetic environment of space. For these reasons, the use of a silicon-based photodetector is better suited for space applications. In this instrument, a Hamamatsu S8664 1010 Si-APD (component 2) was utilized. APDs utilize the photoelectric effect to turn the scintillated light from the crystal into an electronic signal.<sup>9</sup>

Next the preamplifier and shaper, here an Amptek A225 (component 8), receives the signal from the Si-APD, and preserves the energy of the signal in a pulse that initially has the following characteristics: a sharp rise and a long tail with the total signal on the order of microseconds (shown in Fig. 3). Next, because the Amptek A225 acts as a shaper as well, it then takes the signal and cuts down the pulse length to the order of microseconds, preserving the energy as the height of the pulse and changing the shape of the signal to be closer to a Gaussian shape. Next the voltage amplifier, an Amptek 206 (component 9), amplifies the voltage to the pulse. Then the signals outputted by the voltage amplifier go to the MCA, a Kromek K102 (component 7). The MCA measures the Gaussian peaks from the voltage amplifier by pulse height (with the energy value still represented by height, shown in Fig. 3) and sorts pulses by their energy creating an energy spectrum of the interacting events.

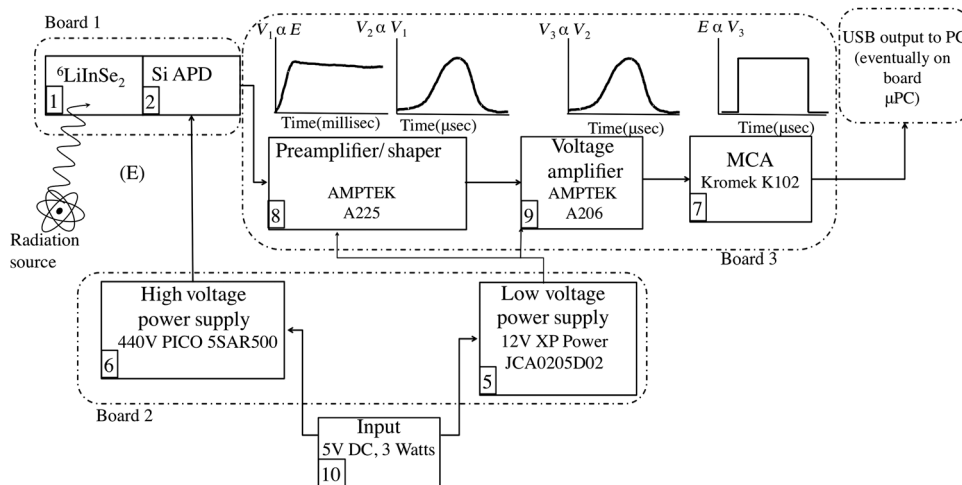


**Fig. 3** Block diagram of the detection system including (1)  $\text{LiInSe}_2$  crystal, (2) Si-APD, (7, 8, 9) associated electronics for signal processing, and (5 and 6) power supplies. The main information extracted from each signal is the height of the pulse, which is linearly proportional to the energy of the ionizing particle detected. Labeling of components is the same used in previous figures.

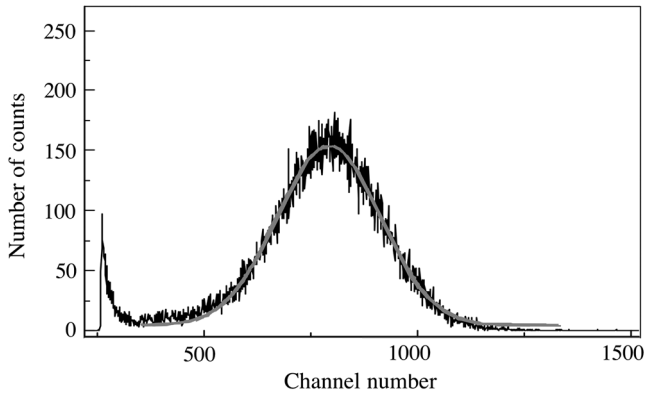


**Fig. 4**  ${}^6\text{LiInSe}_2$  crystal response to alpha radiation from a  ${}^{241}\text{Am}$  source. The spectrum was collected over 100 s.

### 3 Results and Discussion

#### 3.1 ${}^6\text{LiInSe}_2$ Crystal Scintillator

The response to alpha particles is a good indication of the performance of the system before neutron testing. The  ${}^6\text{LiInSe}_2$  crystal was fabricated into a scintillator and its response to alpha radiation from a  ${}^{241}\text{Am}$  source with an activity of  $0.9\ \mu\text{Ci}$  was tested at room temperature before encapsulation and integration into the instrument. The results are shown in Fig. 4.  ${}^{241}\text{Am}$  decays via the emission of an alpha particle with energy 5.486 MeV to  ${}^{237}\text{Np}$  (Neptunium).<sup>16</sup> The energy resolution of 36% was measured as the full width of the distribution at half the maximum of the peak (FWHM). This demonstrates a relatively high signal-to-noise (or signal-to-background) ratio of our system, which means we will approximately be

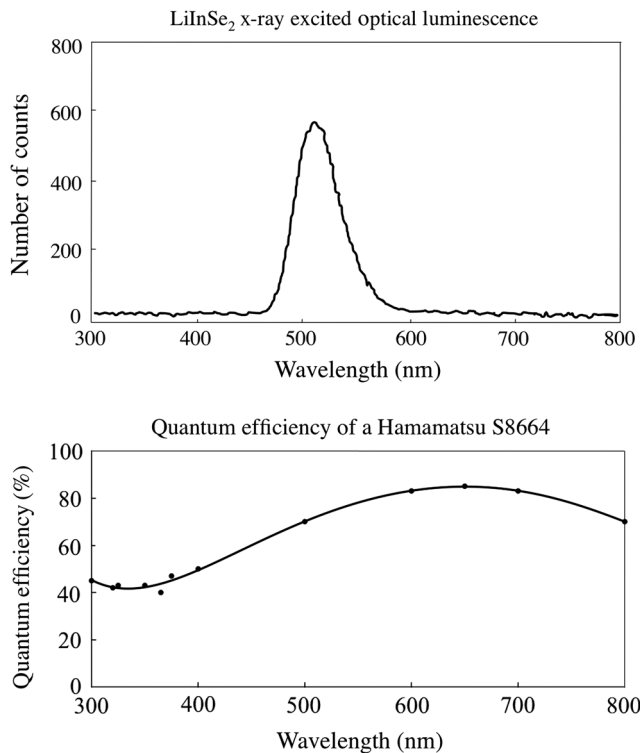


**Fig. 5** Comparison of quantum efficiency of a Hamamatsu S8664 1010 Si-APD and the output spectra of a  ${}^6\text{LiInSe}_2$  crystal.

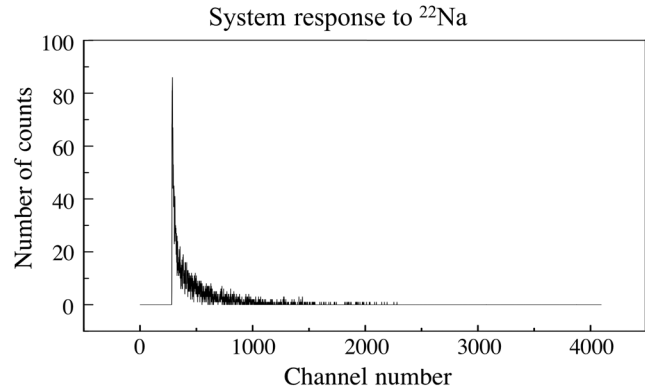


**Fig. 6** Response of packaged instrument to gamma radiation from a  ${}^{22}\text{Na}$  source. Of the 5095 total counts collected, 70% are from direct interaction with the Si-APD.

able to distinguish between two energies separated by 36% or more.<sup>9</sup> The low energy tail that can be seen in Fig. 4 is due to general background, that includes the low energy, 60 KeV, gammas that are generated by this source.

#### 3.2 Silicon Avalanche Photodiode

Available scintillators emit in the blue or ultraviolet parts of the spectrum and, therefore, do not pair as well with silicon-based photodetectors as  ${}^6\text{LiInSe}_2$  does.<sup>12,13,17</sup> This is shown in Fig. 5, where the quantum efficiency of the Hamamatsu S8664, given by the manufacturer, and the emission spectrum of a  ${}^6\text{LiInSe}_2$  crystal, collected using x-ray excited optical luminescence, are shown. It can be seen that the  ${}^6\text{LiInSe}_2$  crystal has its peak emission at about 510 nm, and that the Si-APD has a high efficiency in this range. The blue or UV part of the spectrum, where most other scintillators emit, corresponds to the 400 nm range and lower. From 500 to 400 nm, there is a drop of efficiency from 80% to 40% of the Si-APD. High efficiency in the photodetector is important because  ${}^6\text{LiInSe}_2$  does not have a high light yield, 4400 photons/MeV compared to inorganic and plastic scintillators which have light yields in the 10,000s [e.g., CsI(Tl) has a light yield of 65,000 photons/MeV].<sup>9,12</sup>

#### 3.3 Postassembly System Test

Once the instrument was built, it was tested under gamma radiation. After encapsulation, the system was tested by measuring the response to the 1.2-MeV gammas emitted by  ${}^{22}\text{Na}$ ; the spectrum collected is shown in Fig. 6. The height of the  ${}^{22}\text{Na}$  gamma signal is significantly lower than the response measured to the alpha particles from an  ${}^{241}\text{Am}$  source.

### 4 Conclusions and Future Work

In this study, we have designed and demonstrated a prototype of a neutron detection system packaged into a 1.5-U CubeSat. Weighing 670 g, it can operate on 5 V and has a total power of 3 W, which is considered low and could be supplied by solar panels, and reduces the complexity required for a heat dissipation system. The instruments we are comparing to are 10 to 30 kg and require 15 to 32 W (GRaND and Mars Odyssey).<sup>5,8</sup>

Future steps will include environmental test measurements of the  ${}^6\text{LiInSe}_2$  and Si-APD assembly with a neutron source at the Lunar and Planetary Lab at the University of Arizona and validation of the results using the Monte Carlo N-Particle Transport

Code software package. We are finalizing the experimental setup for epithermal and thermal neutron exposure in a mixed neutron and gamma-ray environment using a Cf-252 source and we will develop an MCPN model that matches the final geometry. This study will be reported in a near-future publication. During these tests, we will utilize the ability of the microcomputer to broadcast data using an antenna to avoid the use of lengthy cables and allow immediate access to collected data while the instrument is under shielding. Testing and characterization of the ability of the instrument to discriminate against gamma-ray events by pulse shape will also be a focus. Our long-term goals for this instrument are to make it self-contained by including a microcomputer and to make it suitable for the environment of space by replacing any components that are not suited for space with radiation hard electronics.<sup>17</sup> This proof of concept instrument was developed and built using only “off the shelf” components.

### Acknowledgments

For helpful feedback and discussion throughout the duration of this project, the authors would like to thank the members of Dr. Burger’s Materials Science and Applications Group and Dr. Stassun’s Astromaterials Group. We also acknowledge the financial support provided by the National Science Foundation through grant #AST-0849736 (PAARE program).

### References

1. J. O. Goldsten, “The NEAR x-ray/gamma-ray spectrometer,” *Johns Hopkins APL Tech. Dig.* **19**(2), 126–135 (1998).
2. P. Jenniskens et al., “The impact and recovery of asteroid 2008TC3,” *Nature* **458**, 485–488 (2009).
3. H. Y. McSween, Jr., *Meteorites and Their Parent Planets*, 2nd ed., Oxford University Press, Oxford (1999).
4. J. G. Bodnarik et al., “Time-resolved neutron/gamma-ray data acquisition for in situ subsurface planetary geochemistry,” *Nucl. Instrum. Methods Phys. Res.* **A707**, 135–142 (2013).
5. W. V. Boynton et al., “The Mars Odyssey gamma-ray spectrometer instrument suite,” *Space Sci. Rev.* **110**(1), 37–83 (2004).
6. W. C. Feldman et al., “Fluxes of fast and epithermal neutrons from lunar prospector: evidence for water ice at the lunar poles,” *Science* **281**(5382), 1496–1500 (1998).
7. A. Parsons et al., “Subsurface *in situ* elemental composition measurements with PING,” in *2013 IEEE Aerospace Conf.*, pp. 1–11 (2013).
8. T. H. Prettyman et al., “Dawn’s Gamma ray and neutron detector,” *Space Sci. Rev.* **163**, 371–459 (2011).
9. G. F. Knoll, *Radiation Detection and Measurement*, John Wiley & Sons, Inc., New Jersey (1979).
10. E. Tupitsyn et al., “Lithium containing chalcogenide single crystals for neutron detection,” *J. Cryst. Growth* **393**, 23–27 (2014).
11. Z. W. Bell et al., “Neutron detection in  $\text{LiInSe}_2$ ,” *Proc. SPIE* **9593**, 95930D (2015).
12. B. Wiggins et al., “Scintillation properties of semiconducting  ${}^6\text{LiInSe}_2$  crystals to ionizing radiation,” *Nucl. Instrum. Methods Phys. Res., Sect. A* **801**, 73–77 (2015).
13. California Polytechnic State University CubeSat Program, “CubeSat,” <http://www.cubesat.org> (2016).
14. J. Nelson et al., “JPL,” <http://www.jpl.nasa.gov/cubesat/missions/iris.php> (2016).
15. A. Klesh and J. Krajewski, “MarCO: CubeSats to Mars in 2016,” in *Paper SSC15-III-3, 29th Annual AIAA/USU Conf. on Small Satellites*, Logan, Utah (2015).
16. *Radioactive Material Safety Data Sheet: Americium-241*, Stuart Hunt and Associates Ltd., St. Albert, Alberta (2001).
17. T. Saito et al., “Astro-H HXI/SGD team, development of high performance avalanche photodiodes and dedicated analog systems for HXI/SGD detectors onboard the Astro-H mission,” *Nucl. Instrum. Methods Phys. Res., Sect. A*, **699**, 230–234 (2013).

Biographies for the authors are not available.